Journal of Systems Engineering and Electronics
Vol. 31, No. 5, October 2020, pp.1031 – 1040

Typical adaptive neural control for hypersonic vehicle based on higher-order filters

ZHAO Hewei[1,*] and LI Rui[2]

1. Shore Guard Institute, Naval Aviation University, Yantai 264001, China;
2. Wenjing College, Yantai University, Yantai 264005, China

Abstract: A typical adaptive neural control methodology is used for the rigid body model of the hypersonic vehicle. The rigid body model is divided into the altitude subsystem and the velocity subsystem. The proportional integral differential (PID) controller is introduced to control the velocity track. The backstepping design is applied for constructing the controllers for the altitude subsystem. To avoid the explosion of differentiation from backstepping, the higher-order filter dynamic is used for replacing the virtual controller in the backstepping design steps. In the design procedure, the radial basis function (RBF) neural network is investigated to approximate the unknown nonlinear functions in the system dynamic of the hypersonic vehicle. The simulations show the effectiveness of the design method.

Keywords: hypersonic vehicle, adaptive neural control, higher-order filter, differential explosion.

DOI: 10.23919/JSEE.2020.000077

1. Introduction

The study of the hypersonic vehicle is important for utilization of the Near Space, which has become a hot issue in recent years. However, there are many challenges to be addressed. One of the challenges is the control system design for the hypersonic vehicle. Many nonlinear control methods and intelligent control methods are used for the design of the control system, moreover, many achievements have been proposed in recent years. It is known that the adaptive backstepping control method can be systematically formulated in a recursive way to achieve the asymptotic stability for a strict feedback system from [1], which is used for the control system design of the hypersonic vehicle in many papers. The adaptive backstepping design based on the nonlinear disturbance observer was proposed in [2], the robustness can be guaranteed and the explosion of differential can be solved by a dynamic surface method. As discussed in [3], the adaptive discrete-time controller was designed via backstepping and the neural network (NN) was used for approximating the known nonlinear functions. The adaptive backstepping method cannot be directly applied when the nonlinear terms in the hypersonic vehicle models are totally unknown or partially unknown. The popular methodology is that the unknown terms are approximated by the NN. The NN methods used in control system design were proposed in many papers [4 – 7]. However, there is a drawback associated with backstepping, the complexity of the control system arising from the repeated differentiations of virtual controllers is difficult to solve, i.e., the so-called differentiation explosion problem. The popular scheme aims to solve such a problem by a filtering instead of the virtual controller differentiations in each backstepping step [8,9]. However, as we know, the stability analysis of the whole closed-loop system consists of the original system and the filter system. It is easy to see that the boundedness of the input of filters and filter dynamics are so important and difficult to establish. So far, there is no systematic methodology to select the control gains and the time constants of the filters. In most papers, the first-order filter is established to solve the explosion problem, moreover, the input of the filter is the virtual controller, and hence the boundedness of filter dynamics is quite involved in the virtual control and the selection of time constants for the filter is important for the stability of the filter. In [10], the higher-order filter was proposed to solve the explosion problem of the backstepping design, and the design parameters are selected to render the polynomial Hurwitz. Therefore, the selection of design parameters can ensure the stability of the filter dynamics.

In this paper, problem formulation will be described in Section 2 which consists of the representation of the dynamic model of the hypersonic vehicle, the control law of the velocity subsystem, and the description of the reference flight path angle. The typical adaptive NN backstepping controller design based on higher-order filters will be pro-

Manuscript received November 16, 2019.
*Corresponding author.
This work was supported by the National Natural Science Foundation of China (61903374).

posed in Section 3. The explosion problem arising from the backstepping method will be avoided by the higher-order filters, moreover, the stability of filter dynamics can be ensured. The stability analysis for the whole closed-loop system will be described in Section 4. In Section 5, to demonstrate its usefulness, simulation will be carried out to verify the effectiveness of the controller proposed. Finally, conclusions and future works are discussed in Section 6.

2. Problem formulation

The longitudinal dynamic model of the hypersonic vehicle in this study was given in [11]. The detail form can be described as follows. There are five rigid-body state variables involved in the model, i.e., V, h, γ, α, Q, while the four flexible state variables are not considered in this study. Moreover, the control inputs are δ_e, i.e., elevator deflection and Φ, i.e., the fuel equivalence ratio.

$$\dot{V} = \frac{1}{m}(T\cos\alpha - D) - g\sin(\theta - \alpha), \tag{1}$$

$$\dot{h} = V\sin(\theta - \alpha), \tag{2}$$

$$\dot{\alpha} = \frac{1}{mV}(-T\sin\alpha - L) + Q + \frac{g}{V}\cos(\theta - \alpha), \tag{3}$$

$$\dot{\theta} = Q, \tag{4}$$

$$I_{yy}\dot{Q} = M, \tag{5}$$

where V is the velocity, h is the altitude, γ is the flight path angle, α is the attack angle, Q is the pitch rate, m is the mass of the aircraft, g is the acceleration due to gravity, θ is the angle of pitch, moreover, T, D, L, M represent the thrust, drag, lift-force, and pitching moment, respectively. And I_{yy} is the moment of inertia about the pitch axis.

The related expressions are described as follows:

$$L = \frac{1}{2}\rho V^2 S C_L, \tag{6}$$

$$D = \frac{1}{2}\rho V^2 S C_D, \tag{7}$$

$$M = z_T T + \frac{1}{2}\rho V^2 S\bar{c}[C_{M,\alpha} + C_{M,\delta_e}], \tag{8}$$

$$T = C_T^{\alpha^3}\alpha^3 + C_T^{\alpha^2}\alpha^2 + C_T^{\alpha}\alpha + C_T^0, \tag{9}$$

where

$$\rho = \rho_0\exp[-(h - h_0)/h_s], \quad C_L = C_L^{\alpha}\alpha + C_L^0,$$

$$C_D = C_D^{\alpha^2}\alpha^2 + C_D^{\alpha}\alpha + C_D^0,$$

$$C_{M,\alpha} = C_{M,\alpha}^{\alpha^2}\alpha^2 + C_{M,\alpha}^{\alpha}\alpha + C_{M,\alpha}^0, \quad C_{M,\delta_e} = c_e\delta_e,$$

$$C_T^{\alpha^3} = \beta_1\Phi + \beta_2, \quad C_T^{\alpha^2} = \beta_3\Phi + \beta_4,$$

$$C_T^{\alpha} = \beta_5\Phi + \beta_6, \quad C_T^0 = \beta_7\Phi + \beta_8.$$

The detail information of parameter values was described in [11]. It is easy to see that $\theta = \alpha + \gamma$, the equations (1) – (5) can be expressed as

$$\begin{cases} \dot{V} = \dfrac{1}{m}(T\cos\alpha - D) - g\sin\gamma \\ \dot{h} = V\sin\gamma \\ \dot{\alpha} = \dfrac{1}{mV}(-T\sin\alpha - L) + Q + \dfrac{g}{V}\cos\gamma \\ \dot{\theta} = Q \\ I_{yy}\dot{Q} = M \end{cases}. \tag{10}$$

The dynamics of model (10) can be divided into two subsystems. One is the velocity subsystem, and the other is the altitude subsystem. For the velocity subsystem, we have

$$\dot{V} = g_V\Phi + f_V \tag{11}$$

where

$$g_V = \frac{1}{m}(\beta_1\alpha^3 + \beta_3\alpha^2 + \beta_5\alpha + \beta_7)\cos\alpha,$$

$$f_V = \frac{1}{m}[(\beta_2\alpha^3 + \beta_4\alpha^2 + \beta_6\alpha + \beta_8)\cdot \cos\alpha - D] - g\sin\gamma.$$

For the velocity subsystem, the control method is not discussed in this study, and the controller is designed directly with the control algorithm form [12], which is in a form of

$$\Phi = k_{pv}z_V + k_{iv}\int z_V\mathrm{d}t + k_{dv}\frac{\mathrm{d}z_V}{\mathrm{d}t} \tag{12}$$

where k_{pv}, k_{iv}, k_{dv} are designed parameters for the proportional integral differential (PID) controller, $z_V = V_r - V$ is the tracking error of velocity, and V_r is the reference velocity.

Based on the timescale conclusion from [13,14], it is obvious that the velocity can be considered as slow dynamic compared with the state variables of the altitude subsystem, therefore the velocity will be treated as constant during the controller design for the altitude subsystem. For the altitude subsystem, the flight path command [15] is designed as

$$\gamma_d = \frac{-k_h(h - h_r) - k_i\displaystyle\int(h - h_r)\mathrm{d}t + \dot{h}_r}{V} \tag{13}$$

where k_h, k_i are positive constants, h_r is the reference altitude. If the flight path angle can follow γ_d, then the altitude tracking error $\widetilde{h} = h - h_r$ can be regulated to zero exponentially. According to [12], we have

$$\dot{\gamma}_d \approx \frac{-k_h(V\sin\gamma - \dot{h}_r) - k_i\widetilde{h} + \ddot{h}_r}{V}. \tag{14}$$

Assumption 1 In (10), it is easy to know that the term $T\sin\alpha$ is generally much smaller than L, which can be neglected.

Define $x_1 = \gamma$, $x_2 = \theta$, $x_3 = Q$, and $\boldsymbol{X} = [x_1, x_2, x_3]^{\mathrm{T}}$, based on Assumption 1, model (10) can be written in a form of

$$\begin{cases} \dot{x}_1 = g_1 x_2 + f_1(x_1) \\ \dot{x}_2 = x_3 \\ \dot{x}_3 = g_3 u + f_3(X) \\ y = x_1 \end{cases} \tag{15}$$

where

$$g_1 = \frac{\rho V S}{2m} C_L^{\alpha},$$

$$f_1 = -\frac{\rho V S}{2m} C_L^{\alpha} x_1 - \frac{g}{V}\cos x_1 + \frac{\rho V S}{2m} C_L^0,$$

$$g_3 = \frac{1}{2I_{yy}} \rho V^2 S \bar{c} c_e,$$

$$f_3 = \frac{z_T T}{I_{yy}} + \frac{1}{2I_{yy}} \rho V^2 S \bar{c} C_{M,\alpha},$$

where $\overline{c}$ is the elevator coefficient and c_e is the canard coefficient.

In (15), $\boldsymbol{X} = [x_1, x_2, x_3]^{\mathrm{T}} \in \mathbf{R}^3$, $u \in \mathbf{R}$, and $y \in \mathbf{R}$ are the state, input and output of the attitude subsystem, respectively. It is obvious that g_1, g_3 are known constants. Without of generality, some assumptions are essential in the sequel.

Assumption 2 The reference output y_d is bounded and smooth.

Assumption 3 The state vector $\boldsymbol{X}$ is measurable.

Assumption 4 The nonlinear functions f_1 and f_3 are unknown and bounded.

For Assumption 1, it is very necessary for establishing the boundedness of signals in the closed-loop system [16,17]. For Assumption 2, the state feedback can be guaranteed, which is needed for the control design. For model (15), it is a strict-feedback form [18], and the backstepping design algorithms can be used to design the controller of the attitude subsystem.

The control goal is that controller u designed in this study for the altitude subsystem and the given controller Φ of the velocity subsystem can steer the altitude and velocity of longitudinal system output dynamics to track the reference values. In this study, the radial basis function (RBF) NN is incorporated with the adaptive method, which will be used for approximating the unknown nonlinear functions. Moreover, the higher-order filter will be used for solving the explosion of the complexity problem from the backstepping design procedure.

3. Controller design

In this section, the classical backstepping method will be developed to design the controller with the higher-order filter solving the differential explosion problems from repeated differentiations of the virtual controllers in each backstepping procedures [19]. The detail steps will be shown in the following.

Step 1 Consider the first case, i.e., $\dot{x}_1 = g_1 x_2 + f_1(x_1)$, then define the tracking error $z_1 = x_1 - y_d$. The direct differentiation for z_1 is

$$\dot{z}_1 = \dot{x}_1 - \dot{y}_d = g_1 x_2 + f_1 - \dot{y}_d. \tag{16}$$

For z_1 dynamic (16), x_2 can be treated as the virtual controller designed for stabilizing the z_1 dynamic. Moreover, the unknown nonlinear function can be approximated by RBF NN [20], which is in a form of

$$g_1^{-1}(f_1 - \dot{y}_d) = \boldsymbol{W}_1^{*\mathrm{T}} \boldsymbol{\phi}_1(\boldsymbol{\vartheta}_1) + \varepsilon_1 \tag{17}$$

where $\boldsymbol{W}_1^*$ is the optimal weight vector, $\boldsymbol{\phi}_1(\boldsymbol{\vartheta}_1)$ is the radical basis function, $\boldsymbol{\vartheta}_1 = [x_1, \dot{y}_d]^{\mathrm{T}}$ is the input vector of NN, and ε_1 is the construction error of NN with the supreme ε_{1m}. Based on (17), we have

$$\dot{z}_1 = g_1(x_2 + \boldsymbol{W}_1^{*\mathrm{T}} \boldsymbol{\phi}_1 + \varepsilon_1). \tag{18}$$

Define the second tracking error $z_2 = x_2 - x_{2v}$, and the virtual controller x_{2v} is proposed in a form of

$$x_{2v} = -k_1 z_1 - \widehat{\boldsymbol{W}}_1^{\mathrm{T}} \boldsymbol{\phi}_1 - \widehat{\varepsilon}_1 \tanh\left(\frac{z_1}{\delta}\right) \tag{19}$$

where $k_1 > 0$ is the design parameter, δ is a positive constant [21], $\widehat{\boldsymbol{W}}_1$ is the estimation of $\boldsymbol{W}_1^*$, and $\widehat{\varepsilon}_1$ is the estimation of ε_{1m}, moreover, we can define the errors $\widetilde{\boldsymbol{W}}_1 = \boldsymbol{W}_1^* - \widehat{\boldsymbol{W}}_1$, $\widetilde{\varepsilon}_1 = \varepsilon_{1m} - \widehat{\varepsilon}_1$. By substituting (19) into (18), it yields

$$\dot{z}_1 = g_1 \Bigg[-k_1 z_1 + z_2 + \widetilde{\boldsymbol{W}}_1^{\mathrm{T}} \boldsymbol{\phi}_1 + \widetilde{\varepsilon}_1 \tanh\left(\frac{z_1}{\delta}\right) + \varepsilon_1 - \varepsilon_{1m} \tanh\left(\frac{z_1}{\delta}\right) \Bigg]. \tag{20}$$

A Lyapunov function is constructed in a form of

$$L_1 = \frac{1}{2g_1} z_1^2 + \frac{1}{2} \widetilde{\boldsymbol{W}}_1^{\mathrm{T}} \Gamma_1^{-1} \widetilde{\boldsymbol{W}}_1 + \frac{1}{2\varpi_1} \widetilde{\varepsilon}_1^2 \tag{21}$$

where Γ_1, ϖ_1 are positive design parameters. By a direct differentiation of (21), it yields

$$\dot{L}_1 = \frac{1}{g_1} \dot{z}_1 z_1 + \dot{\widetilde{\boldsymbol{W}}}_1^{\mathrm{T}} \Gamma_1^{-1} \widetilde{\boldsymbol{W}}_1 + \frac{1}{\varpi_1} \dot{\widetilde{\varepsilon}}_1 \widetilde{\varepsilon}_1 = z_1 \Bigg[-k_1 z_1 + z_2 + \widetilde{\boldsymbol{W}}_1^{\mathrm{T}} \boldsymbol{\phi}_1 + \widetilde{\varepsilon}_1 \tanh\left(\frac{z_1}{\delta}\right) + \varepsilon_1 - \varepsilon_{1m} \tanh\left(\frac{z_1}{\delta}\right) \Bigg] - \dot{\widehat{\boldsymbol{W}}}_1^{\mathrm{T}} \Gamma_1^{-1} \widetilde{\boldsymbol{W}}_1 - \frac{1}{\varpi_1} \dot{\widehat{\varepsilon}}_1 \widetilde{\varepsilon}_1. \tag{22}$$

The updating laws for $\widehat{\boldsymbol{W}}_1$, $\widehat{\varepsilon}_1$, respectively, can be designed as follows:

$$\begin{cases} \dot{\widehat{\boldsymbol{W}}}_1 = \Gamma_1(z_1\boldsymbol{\phi}_1 - \lambda_1\widehat{\boldsymbol{W}}_1) \\ \dot{\widehat{\varepsilon}}_1 = \varpi_1\left[z_1\tanh\left(\dfrac{z_1}{\delta}\right) - \sigma_1\widehat{\varepsilon}_1\right] \end{cases} \tag{23}$$

where λ_1, σ_1 are the positive design parameters. Substituting the updating algorithm (23) into (22), it yields

$$\dot{L}_1 = -k_1z_1^2 + z_1z_2 + z_1\left[\varepsilon_1 - \varepsilon_{1m}\tanh\left(\frac{z_1}{\delta}\right)\right] + \lambda_1\widehat{\boldsymbol{W}}_1^{\mathrm{T}}\widetilde{\boldsymbol{W}}_1 + \sigma_1\widehat{\varepsilon}_1\widetilde{\varepsilon}_1. \tag{24}$$

Step 2 The differentiation z_2 is calculated as

$$\dot{z}_2 = \dot{x}_2 - \dot{x}_{2v} = x_3 - \dot{x}_{2v}. \tag{25}$$

Clearly, the differentiation of the virtual controller x_{2v} is so difficult to calculate and the explosion of the complexity problem is unfavorable to the practical implementation [22]. Thus in this section, the differentiation of x_{2v} is replaced with filtering to conquer the explosion problem. Then let x_{2v} pass through an $(n-1)$th-order filter in a form of

$$\sum_{i=0}^{n-1}\eta_{2,i}q_2^{(i)} = x_{2v}, \quad q_2(0) = x_{2v}(0) \tag{26}$$

where n is the order number of the system, $\eta_{2,i}$ is the positive number chosen to render the polynomial $\eta_{2,n-1}s^{n-1} + \eta_{2,n-2}s^{n-2} + \cdots + \eta_{2,0}$ Hurwitz, i.e., $\eta_{2,2}\ddot{q}_2 + \eta_{2,1}\dot{q}_2 + \eta_{2,0}q_2 = x_{2v}, q_2(0) = x_{2v}(0)$. Based on the results from [6], x_{2v} can be replaced with the output q_2 of filter (26), i.e., $x_{2v} = q_2$, and $\dot{x}_{2v} = \dot{q}_2$.

Remark 1 The reason for using a higher-order filter instead of a typical general first-order filter is that the output of the filter (26) is involved in the next virtual controller. It is easy to see that the virtual controller (19) is bounded, and based on the higher-order design algorithm, stability of the filter (26) dynamics can be ensured, then the output of the filter (26) is bounded, which is an important issue for the boundedness of the next virtual controller.

Based on the result above, the explosion of the complexity problem arising from the differentiation of the virtual controller (19) can be avoided. To this end, we have

$$\dot{z}_2 = \dot{x}_2 - \dot{x}_{2v} = x_3 - \dot{q}_2. \tag{27}$$

Likewise, for z_2 dynamic, x_3 can be treated as the virtual controller designed for stabilizing equilibrium $z_2 = 0$. Define the tracking error $z_3 = x_3 - x_{3v}$, the virtual controller x_{3v} can be proposed as

$$x_{3v} = -k_2z_2 - z_1 + \dot{q}_2 \tag{28}$$

where k_2 is the positive design parameter. Substituting (28) into (27), it yields

$$\dot{z}_2 = z_3 + x_{3v} - \dot{q}_2 = -k_2z_2 - z_1 + z_3. \tag{29}$$

Consider the following Lyapunov function

$$L_2 = \frac{1}{2}z_2^2. \tag{30}$$

The differentiation of (30) is calculated as

$$\dot{L}_2 = \dot{z}_2z_2 = -k_2z_2^2 - z_1z_2 + z_2z_3. \tag{31}$$

Step 3 The differentiation of z_3 is attained as follows:

$$\dot{z}_3 = \dot{x}_3 - \dot{x}_{3v}. \tag{32}$$

Likewise, let x_{3v} pass a higher-order filter, which can be replaced with the output of the filter, i.e., $\dot{x}_{3v} = \dot{q}_3$. The higher-order filter is in a form of

$$\sum_{i=0}^{n-2}\eta_{3,i}q_3^{(i)} = x_{3v}, \quad q_3(0) = x_{3v}(0) \tag{33}$$

where $\eta_{3,i}$ is the positive number chosen to render the polynomial $\eta_{3,n-1}s^{n-1} + \eta_{3,n-2}s^{n-2} + \cdots + \eta_{3,0}$ Hurwitz, i.e., $\eta_{3,1}\dot{q}_3 + \eta_{3,0}q_3 = x_{3v}, q_3(0) = x_{3v}(0)$.

Remark 2 Clearly, the virtual controller x_{3v} is bounded, moreover, it is the input of the filter (33), then the dynamics stability of the filter (33) can be ensured, i.e., q_3 is bounded, which is involved in the next controller.

Substituting $\dot{x}_3$ of (15) into (32), it yields

$$\dot{z}_3 = g_3u + f_3(X) - \dot{q}_3. \tag{34}$$

The unknown nonlinear function $f_3(\boldsymbol{X})$ can be approximated by RBF NN, which is in a form of

$$f_3(\boldsymbol{X}) = \boldsymbol{W}_3^{*\mathrm{T}}\boldsymbol{\phi}_3(\boldsymbol{\vartheta}_3) + \varepsilon_3 \tag{35}$$

where $\boldsymbol{W}_3^*$ is the optimal weight vector, $\boldsymbol{\phi}_3(\boldsymbol{\vartheta}_3)$ is the radical basis function, $\boldsymbol{\vartheta}_3 = [x_1, x_2, x_3]^{\mathrm{T}}$ is the input vector of NN, and ε_3 is the construction error of NN with the supreme ε_{3m}. Based on (35), we have

$$\dot{z}_3 = g_3u + \boldsymbol{W}_3^{*\mathrm{T}}\boldsymbol{\phi}_3(\boldsymbol{\vartheta}_3) + \varepsilon_3 - \dot{q}_3. \tag{36}$$

Clearly, the overall controller of the system, i.e., u, is proposed in a form of

$$u = g_3^{-1}\left[-k_3z_3 - z_2 - \widehat{\boldsymbol{W}}_3^{\mathrm{T}}\boldsymbol{\phi}_3 - \widehat{\varepsilon}_3\tanh\left(\frac{z_3}{\delta}\right) + \dot{q}_3\right] \tag{37}$$

where k_3 is a positive design parameter, δ is a positive constant, likewise, define errors $\widetilde{\boldsymbol{W}}_3 = \boldsymbol{W}_3^* - \widehat{\boldsymbol{W}}_3$, $\widetilde{\varepsilon}_3 = \varepsilon_{3m} - \widehat{\varepsilon}_3$. It is easy to see that $\dot{q}_3$ is in the overall controller,

while based on Remark 2, $\dot{q}_3$ is bounded. Substituting (37) into (36), we have

$$\dot{z}_3 = -k_3 z_3 - z_2 + \widetilde{\boldsymbol{W}}_3^{\mathrm{T}}\boldsymbol{\phi}_3 + \widetilde{\varepsilon}_3 \tanh\left(\frac{z_3}{\delta}\right) + \varepsilon_3 - \varepsilon_{3m}\tanh\left(\frac{z_3}{\delta}\right). \tag{38}$$

Consider the following Lyapunov function:

$$L_3 = \frac{1}{2}z_3^2 + \frac{1}{2}\widetilde{\boldsymbol{W}}_3^{\mathrm{T}}\Gamma_3^{-1}\widetilde{\boldsymbol{W}}_3 + \frac{1}{2\varpi_3}\widetilde{\varepsilon}_3^2. \tag{39}$$

The direct differentiation of (39) is calculated as

$$\dot{L}_3 = \dot{z}_3 z_3 + \dot{\widetilde{\boldsymbol{W}}}_3^{\mathrm{T}}\Gamma_3^{-1}\widetilde{\boldsymbol{W}}_3 + \frac{1}{\varpi_3}\dot{\widetilde{\varepsilon}}_3\widetilde{\varepsilon}_3 = \dot{z}_3 z_3 - \dot{\widehat{\boldsymbol{W}}}_3^{\mathrm{T}}\Gamma_3^{-1}\widetilde{\boldsymbol{W}}_3 - \frac{1}{\varpi_3}\dot{\widehat{\varepsilon}}_3\widetilde{\varepsilon}_3. \tag{40}$$

Substituting (38) into (40), it yields

$$\dot{L}_3 = -k_3 z_3^2 - z_2 z_3 + z_3\left[\varepsilon_3 - \varepsilon_{3m}\tanh\left(\frac{z_3}{\delta}\right)\right] + z_3\left[\widetilde{\boldsymbol{W}}_3^{\mathrm{T}}\boldsymbol{\phi}_3 + \widetilde{\varepsilon}_3\tanh\left(\frac{z_3}{\delta}\right)\right] - \dot{\widehat{\boldsymbol{W}}}_3^{\mathrm{T}}\Gamma_3^{-1}\widetilde{\boldsymbol{W}}_3 - \frac{1}{\varpi_3}\dot{\widehat{\varepsilon}}_3\widetilde{\varepsilon}_3. \tag{41}$$

The updating algorithms can be designed as follows:

$$\begin{cases} \dot{\widehat{\boldsymbol{W}}}_3 = \Gamma_3(z_3\boldsymbol{\phi}_3 - \lambda_3\widehat{\boldsymbol{W}}_3) \\ \dot{\widehat{\varepsilon}}_3 = \varpi_3\left[z_3\tanh\left(\frac{z_3}{\delta}\right) - \sigma_3\widehat{\varepsilon}_3\right] \end{cases} \tag{42}$$

where λ_3, σ_3 are the positive design parameters. Then substituting updating laws (42) into (41), it yields

$$\dot{L}_3 = -k_3 z_3^2 - z_2 z_3 + z_3\left[\varepsilon_3 - \varepsilon_{3m}\tanh\left(\frac{z_3}{\delta}\right)\right] + \lambda_3\widehat{\boldsymbol{W}}_3^{\mathrm{T}}\widetilde{\boldsymbol{W}}_3 + \sigma_3\widehat{\varepsilon}_3\widetilde{\varepsilon}_3. \tag{43}$$

4. Stability analysis

As mentioned, the notion of input-state-stability (ISS) has been utilized in the controller design of nonlinear systems in recent years. ISS means that the bounded input implies the bounded state [16]. In this section, the stability of the control system designed is verified in two steps. Firstly, the ISS stability will be analyzed. Besides, the Lyapunov stability method [23–25] will be used for verifying that all the states of the closed-loop control system are uniformly ultimately bounded [26,27].

Theorem 1 For the closed-loop control system consisting of the plant (15), virtual controllers (19) and (28), overall controller (37), and the NN adaptive tuning laws (23) and (42) are designed. If the control gain and tuning parameters can be selected reasonably, all the signals in the closed-loop system are uniformly ultimately bounded. Besides, tracking errors can converge uniformly to the following set Ω, and the radius can be controlled arbitrarily small with the sufficiently large design parameters. The relative definitions will be given later.

$$\Omega \triangleq \{z_1, z_2, z_3, \widetilde{\boldsymbol{W}}_1, \widetilde{\boldsymbol{W}}_3, \widetilde{\varepsilon}_1, \widetilde{\varepsilon}_3 \big| |z_1|^2 \leqslant 2g_1 L(0) + \frac{2g_1 C}{\zeta}, |z_2|^2 \leqslant 2L(0) + \frac{2C}{\zeta}, |z_3|^2 \leqslant 2L(0) + \frac{2C}{\zeta}, \|\widetilde{\boldsymbol{W}}_1\|^2 \leqslant \frac{2L(0)}{\lambda_{\min}(\Gamma_1^{-1})} + \frac{2C}{\zeta\lambda_{\min}(\Gamma_1^{-1})}, \|\widetilde{\boldsymbol{W}}_3\|^2 \leqslant \frac{2L(0)}{\lambda_{\min}(\Gamma_3^{-1})} + \frac{2C}{\zeta\lambda_{\min}(\Gamma_3^{-1})}, |\varepsilon_1|^2 \leqslant 2L(0) + \frac{2C}{\zeta}, |\varepsilon_3|^2 \leqslant 2L(0) + \frac{2C}{\zeta}\}$$

For the proposed control system consists of two subsystems, i.e., the filter closely system, and the original error system, the stability of the whole closely system needs two sides. One is the output boundedness of filters, and the other is the boundedness of original error system signals.

Proof It is easy to know that (23) is bounded, which in turn can ensure the boundedness of virtual control law (19). In (26), the virtual controller is the input of the filter (26), clearly, the boundedness of the virtual controller (19) implies the boundedness of output state q_2 from the filter (26). Output state q_2 of the filter (26) is the component of virtual controller (28). Thus. it is easy to see that the virtual controller (28) is bounded, which is the input of the filter (33), and can ensure the bounded stability of the constructed filter dynamics, in turn q_3 is bounded, which is the component of the overall controller (37). Besides, based on the boundedness of (42), the overall control input (37) is bounded, we can know that all state signals of the original error system are bounded, and the design filters dynamics are bounded, then the whole closed-loop system is ISS. The two systems are coupling through the above analysis, thus the boundedness needs to be verified for the two systems. Then the uniform ultimately bounded will be analyzed with Lyapunov stability methods.

Consider the Lyapunov function in a form of

$$L = L_1 + L_2 + L_3 \tag{44}$$

where

$$L_1 = \frac{1}{2g_1}z_1^2 + \frac{1}{2}\widetilde{\boldsymbol{W}}_1^{\mathrm{T}}\Gamma_1^{-1}\widetilde{\boldsymbol{W}}_1 + \frac{1}{2\varpi_1}\widetilde{\varepsilon}_1^2,$$

$$L_2 = \frac{1}{2}z_2^2,$$

$$L_3=\frac{1}{2}z_3^2+\frac{1}{2}\widetilde{\boldsymbol{W}}_3^{\mathrm{T}}\Gamma_3^{-1}\widetilde{\boldsymbol{W}}_3+\frac{1}{2\varpi_3}\widetilde{\varepsilon}_3^2.$$

Differentiating (44) along (24), (31) and (43), we have

$$\begin{aligned}\dot{L}=\dot{L}_1+\dot{L}_2+\dot{L}_3=\\ -k_1z_1^2-k_2z_2^2-k_3z_3^2+\lambda_1\widehat{\boldsymbol{W}}_1^{\mathrm{T}}\widetilde{\boldsymbol{W}}_1+\\ \sigma_1\widehat{\varepsilon}_1\widetilde{\varepsilon}_1+\lambda_3\widehat{\boldsymbol{W}}_3^{\mathrm{T}}\widetilde{\boldsymbol{W}}_3+\sigma_3\widehat{\varepsilon}_3\widetilde{\varepsilon}_3+\\ z_1\left[\varepsilon_1-\varepsilon_{1m}\tanh\left(\frac{z_1}{\delta}\right)\right]+z_3\left[\varepsilon_3-\varepsilon_{3m}\tanh\left(\frac{z_3}{\delta}\right)\right].\end{aligned}\tag{45}$$

For easy reference, we quote the following inequalities [28 – 30]:

$$\begin{cases}\widehat{\boldsymbol{W}}_1^{\mathrm{T}}\widetilde{\boldsymbol{W}}_1\leqslant\dfrac{1}{2}\|\boldsymbol{W}_1^*\|^2-\dfrac{1}{2}\|\widetilde{\boldsymbol{W}}_1\|^2\\ \widehat{\boldsymbol{W}}_3^{\mathrm{T}}\widetilde{\boldsymbol{W}}_3\leqslant\dfrac{1}{2}\|\boldsymbol{W}_3^*\|^2-\dfrac{1}{2}\|\widetilde{\boldsymbol{W}}_3\|^2\\ \widehat{\varepsilon}_1\widetilde{\varepsilon}_1\leqslant\dfrac{1}{2}\varepsilon_{1m}^2-\dfrac{1}{2}\widetilde{\varepsilon}_1^2\\ \widehat{\varepsilon}_3\widetilde{\varepsilon}_3\leqslant\dfrac{1}{2}\varepsilon_{3m}^2-\dfrac{1}{2}\widetilde{\varepsilon}_3^2\end{cases}.\tag{46}$$

The following inequalities can be attained:

$$\begin{aligned}\dot{L}\leqslant-k_1z_1^2-k_2z_2^2-k_3z_3^2+\frac{1}{2}\lambda_1\|\boldsymbol{W}_1^*\|^2-\\ \frac{1}{2}\lambda_1\|\widetilde{\boldsymbol{W}}_1\|^2+\frac{1}{2}\sigma_1\varepsilon_{1m}^2-\frac{1}{2}\sigma_1\widetilde{\varepsilon}_1^2+\\ \frac{1}{2}\lambda_3\|\boldsymbol{W}_3^*\|^2-\frac{1}{2}\lambda_3\|\widetilde{\boldsymbol{W}}_3\|^2+\frac{1}{2}\sigma_3\varepsilon_{3m}^2-\\ \frac{1}{2}\sigma_3\widetilde{\varepsilon}_3^2+z_1\left[\varepsilon_1-\varepsilon_{1m}\tanh\left(\frac{z_1}{\delta}\right)\right]+\\ z_3\left[\varepsilon_3-\varepsilon_{3m}\tanh\left(\frac{z_3}{\delta}\right)\right].\end{aligned}\tag{47}$$

Based on the results from [17], the following inequality holds:

$$0\leqslant|\eta|-\eta\tanh(\frac{\eta}{\delta})\leqslant c_\eta\delta,\quad\eta\in\mathbf{R}\tag{48}$$

where c_η is selected as 0.278 5. It is easy to verify that the above-mentioned inequality is very useful for the stability analysis.

Hence according to (48), we know

$$\begin{aligned}\varepsilon_1z_1-\varepsilon_{1m}z_1\tanh\left(\frac{z_1}{\delta}\right)\leqslant\\ \varepsilon_{1m}|z_1|-\varepsilon_{1m}z_1\tanh\left(\frac{z_1}{\delta}\right)\leqslant\\ \varepsilon_{1m}\left[|z_1|-z_1\tanh\left(\frac{z_1}{\delta}\right)\right]\leqslant\varepsilon_{1m}c_\eta\delta.\end{aligned}\tag{49}$$

Likewise we have

$$\varepsilon_3z_3-\varepsilon_{3m}z_3\tanh\left(\frac{z_3}{\delta}\right)\leqslant\varepsilon_{3m}c_\eta\delta.\tag{50}$$

Substituting (49), (50) into (47) yields

$$\begin{aligned}\dot{L}\leqslant-k_1z_1^2-k_2z_2^2-k_3z_3^2+\frac{1}{2}\lambda_1\|\boldsymbol{W}_1^*\|^2-\\ \frac{1}{2}\lambda_1\|\widetilde{\boldsymbol{W}}_1\|^2+\frac{1}{2}\sigma_1\varepsilon_{1m}^2-\frac{1}{2}\sigma_1\widetilde{\varepsilon}_1^2+\\ \frac{1}{2}\lambda_3\|\boldsymbol{W}_3^*\|^2-\frac{1}{2}\lambda_3\|\widetilde{\boldsymbol{W}}_3\|^2+\frac{1}{2}\sigma_3\varepsilon_{3m}^2-\\ \frac{1}{2}\sigma_3\widetilde{\varepsilon}_3^2+(\varepsilon_{1m}+\varepsilon_{3m})c_\eta\delta.\end{aligned}\tag{51}$$

Considering (21), (30) and (39), we have

$$\dot{L}\leqslant-\sum_{i=1}^{3}\zeta_iL_i+C\tag{52}$$

with

$$\begin{aligned}\zeta_1=\min\left[2k_1g_1,\frac{\lambda_1}{\lambda_{\max}(\Gamma_1^{-1})},\sigma_1\varpi_1\right],\quad\zeta_2=2k_2,\\ \zeta_3=\min\left[2k_3,\frac{\lambda_3}{\lambda_{\max}(\Gamma_3^{-1})},\sigma_3\varpi_3\right],\\ C=\frac{1}{2}\lambda_1\|\boldsymbol{W}_1^*\|^2+\frac{1}{2}\lambda_3\|\boldsymbol{W}_3^*\|^2+\frac{1}{2}\sigma_1\varepsilon_{1m}^2+\\ \frac{1}{2}\sigma_3\varepsilon_{3m}^2+(\varepsilon_{1m}+\varepsilon_{3m})c_\eta\delta.\end{aligned}$$

The conclusion is attained as follows:

$$\dot{L}\leqslant-\zeta L+C\tag{53}$$

with $\zeta=\min[\zeta_1,\zeta_2,\zeta_3]$. It is easy to know that C is a bounded constant.

Based on (49), we have

$$L\leqslant L(0)\mathrm{e}^{-\zeta t}+\frac{C}{\zeta}\leqslant L(0)+\frac{C}{\zeta},\quad\forall t\geqslant0.\tag{54}$$

Besides considering (44), we can obtain the conclusion that all signals of the closed-loop system are bounded, moreover, the tracking errors can be converted into a bounded invariant set as follows:

$$\begin{aligned}\Omega\triangleq\{z_1,z_2,z_3,\widetilde{\boldsymbol{W}}_1,\widetilde{\boldsymbol{W}}_3,\widetilde{\varepsilon}_1,\widetilde{\varepsilon}_3\big||z_1|^2\leqslant2g_1L(0)+\frac{2g_1C}{\zeta},\\ |z_2|^2\leqslant2L(0)+\frac{2C}{\zeta};|z_3|^2\leqslant2L(0)+\frac{2C}{\zeta};\\ \|\widetilde{\boldsymbol{W}}_1\|^2\leqslant\frac{2L(0)}{\lambda_{\min}(\Gamma_1^{-1})}+\frac{2C}{\zeta\lambda_{\min}(\Gamma_1^{-1})};\\ \|\widetilde{\boldsymbol{W}}_3\|^2\leqslant\frac{2L(0)}{\lambda_{\min}(\Gamma_3^{-1})}+\frac{2C}{\zeta\lambda_{\min}(\Gamma_3^{-1})};\end{aligned}$$

$$|\varepsilon_1|^2 \leqslant 2L(0) + \frac{2C}{\zeta}; |\varepsilon_3|^2 \leqslant 2L(0) + \frac{2C}{\zeta}\}. \quad (55)$$

5. Simulations

In this section, the effectiveness of control system design strategies will be proved through simulation. The control gains are selected as $k_1 = 18$, $k_2 = 7$, $k_3 = 10$, $k_h = 0.3$, $k_i = 0.1$, $k_{pv} = 0.5$, $k_{iv} = 7$, $k_{dv} = 10$. Moreover, the updating laws parameters are selected as $\Gamma_1 = 5$, $\lambda_1 = 0.001$, $\varpi_1 = 15$, $\sigma_1 = 2.5$, $\Gamma_3 = 2.5$, $\lambda_3 = 0.001$, $\varpi_3 = 0.01$, $\sigma_3 = 0.002$, $\delta = 0.05$. And the higher-order filters parameters can be designed as $\eta_{2,2} = 2$, $\eta_{2,1} = 1$, $\eta_{2,0} = 1$, $\eta_{3,1} = 1$, $\eta_{3,0} = 0.05$. The numbers of NN nodes are selected as $N_1 = 20$ and $N_2 = 20$, with their centers being evenly spaced in $[-0.5, 0.5] \times [-0.5, 0.5]$ and $[-0.5, 0.5] \times [-9.7, 9.7] \times [-4.5, 4.5]$, respectively.

In simulation, the reference altitude h_r of altitude subsystem simulation is achieved through a filter presented as follows:

$$\frac{h_r}{h_c} = \frac{0.5 \times 0.2^2}{(s + 0.5)(s^2 + 2 \times 0.9 \times 0.2s + 0.2^2)}$$

where h_c is the command signal, which climbs from 85 000 ft to 87 000 ft in 40 s, and then descends to 86 000 ft. The reference velocity V_r of the velocity subsystem simulation is achieved through a filter presented as follows:

$$\frac{V_r}{V_c} = \frac{0.3 \times 0.2^2}{(s + 0.3)(s^2 + 2 \times 0.7 \times 0.2s + 0.2^2)}$$

where V_c is the command signal, which climbs from 8 850 ft/s to 8 900 ft/s in 20 s, and then climbs to 9 150 ft/s.

The initial condition of simulation is shown in Table 1. The simulation results are shown in figures that follow.

Table 1 The initial values

State	Value	Unit
h	85 000	ft
V	8 850	ft/s
γ	0	°
θ	0	°
Q	0	(°)/s

In Fig. 1, we can see that the altitude tracks the reference signal well. The altitude tracking error is shown in Fig. 2, and the results can illustrate that the altitude subsystem design is satisfied. As shown in Fig. 3, the flight velocity can track the reference signal well, moreover, the result, i.e., the velocity tracking error from Fig. 4 can indicate that the PID contrller can fulfill the velocity tracking task.

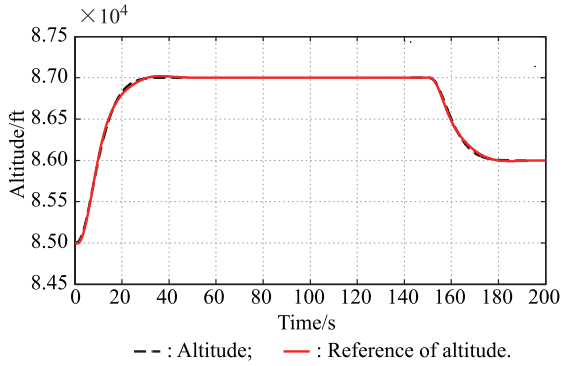

Fig. 1 Altitude tracking

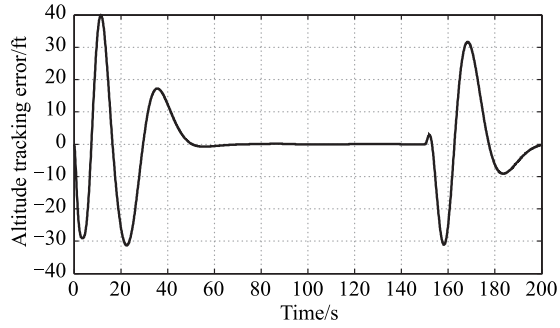

Fig. 2 Altitude tracking error

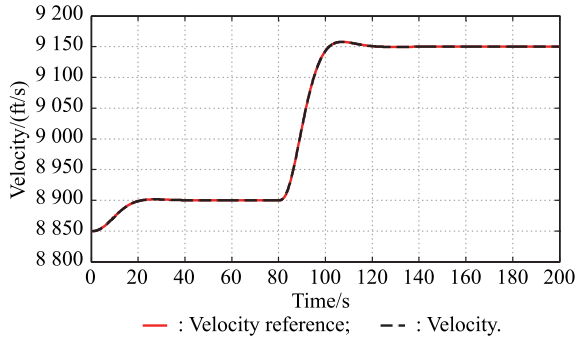

Fig. 3 Velocity tracking

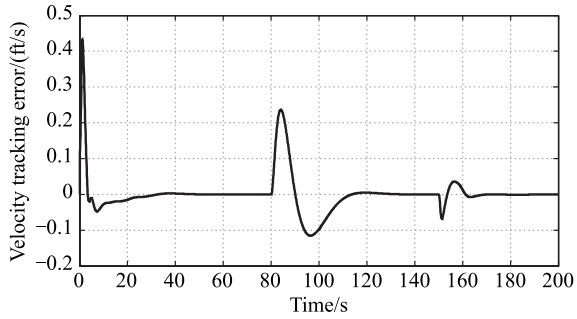

Fig. 4 Velocity tracking error

The elevator deflection is shown in Fig. 5. It is easy to see that the input of the altitude subsystem is bounded and smooth. The virtual controllers of the altitude subsystem are shown in Fig. 6 and Fig. 7. The input of the velocity subsystem, i.e., the fuel equivalence raio is shown in

Fig. 8, which is bounded within (0,1.2). From Fig. 9 to Fig. 11, the altitude subsystem states, i.e., the flight path angle, the angle of pitch, and the pitch rate, are bounded. The tracking errors of system states can be demonstrated in Fig. 12.

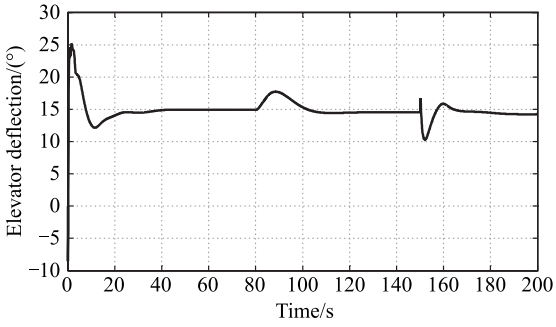

Fig. 5 Elevator deflection

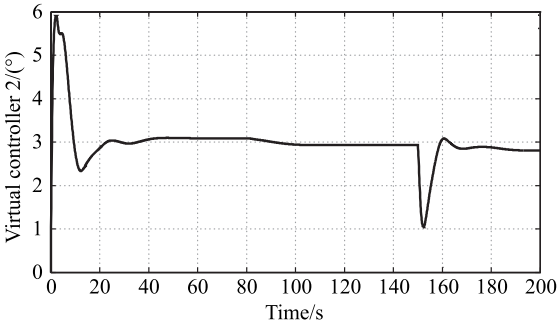

Fig. 6 Virtual controller x_{2v}

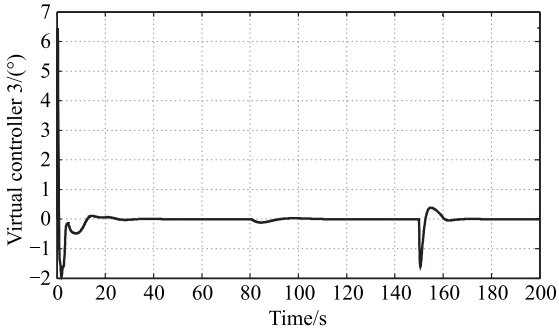

Fig. 7 Virtual controller x_{3v}

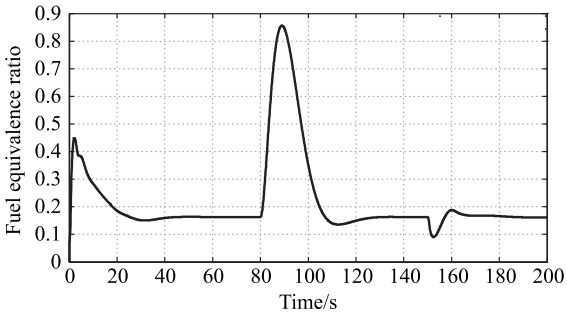

Fig. 8 Fuel equivalence ratio

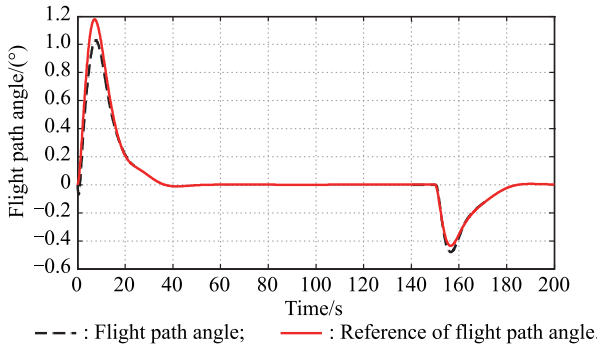

Fig. 9 Flight path angle

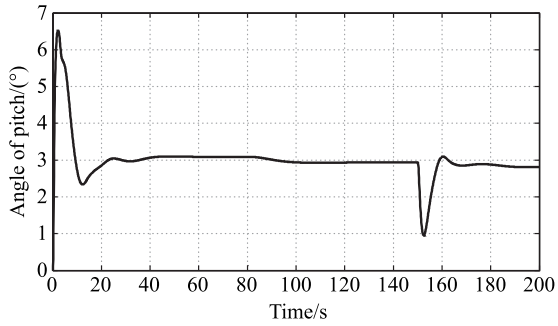

Fig. 10 Angle of pitch

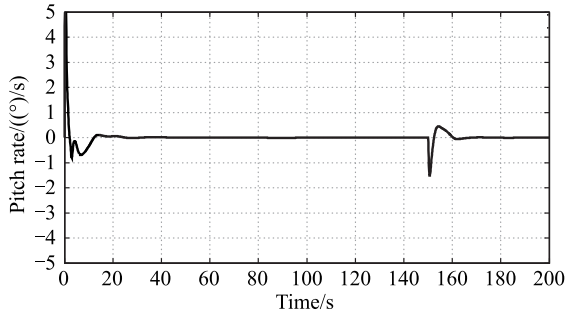

Fig. 11 Pitch rate

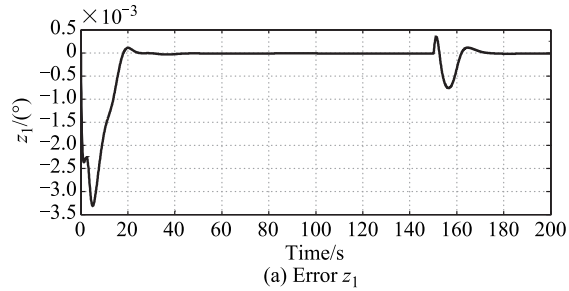

(a) Error z_1

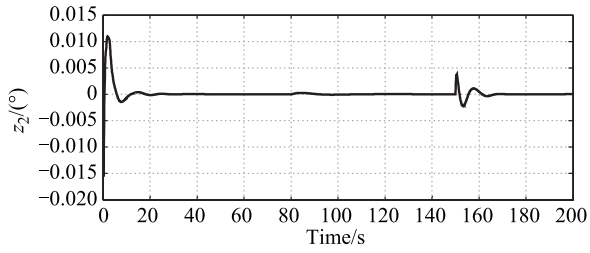

(b) Error z_2

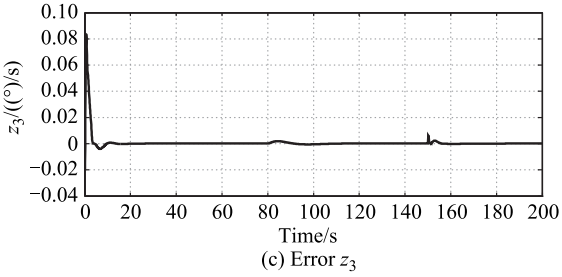

(c) Error z_3

Fig. 12 System states tracking errors

The filter dynamics q_2 and q_3 are represented in Fig. 13 and Fig. 14. It is obvious that the fitler dynamics are bounded and smooth, thus the filters design is effective.

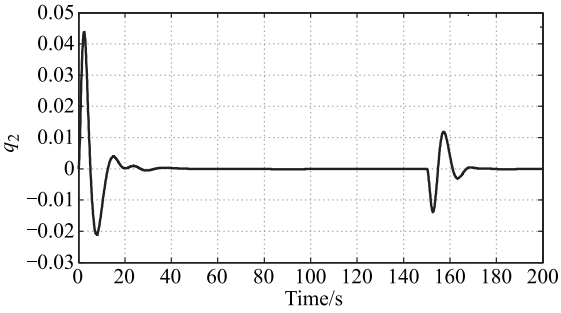

Fig. 13 Filter dynamic q_2

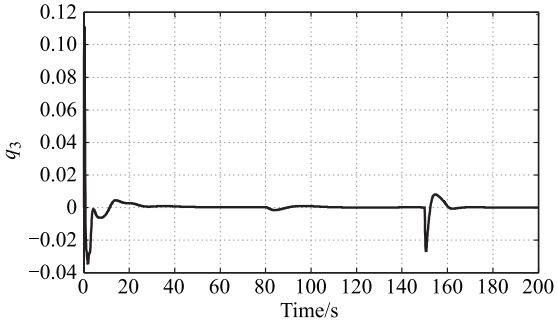

Fig. 14 Filter dynamic q_3

The estimations of NN weights in Fig. 15 are smooth, and the NN approximations for unknown nonlinear functions f_1 and f_3 are shown in Fig. 16 and Fig. 17. The approximation performance could satisfy the requirement for the control system design.

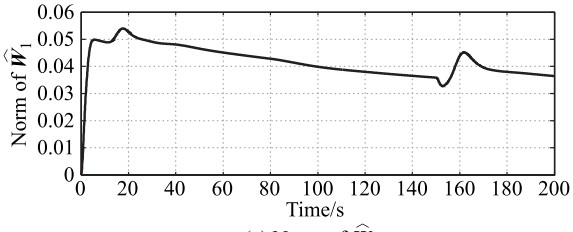

(a) Norm of $\widehat{W}_1$

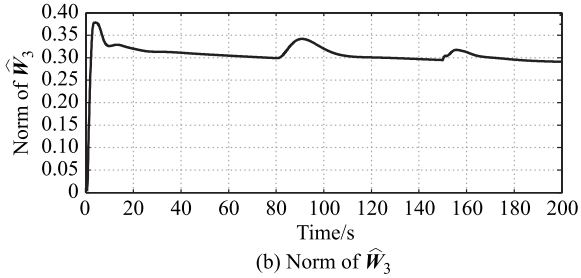

(b) Norm of $\widehat{W}_3$

Fig. 15 Norm of $\widehat{W}_1$ and $\widehat{W}_3$

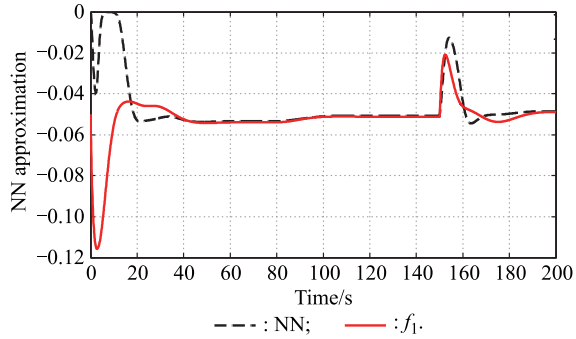

Fig. 16 NN approximation for f_1

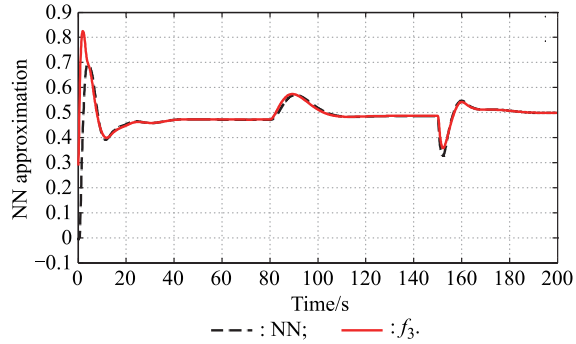

Fig. 17 NN approximation for f_3

6. Conclusions

The typical adaptive neural control involved in the backstepping method is applied for the control system design of the hypersonic vehicle in this paper. Moreover, the higher-order filters are used for avoiding the explosions of differentiation in backstepping steps. The important issue is that the design parameter of higher-order filter selection methodology is proposed. The NN can be improved in the future work, since the range of RBF function action is limited, and NN cannot approximate the unknown nonlinear functions when the dynamics are out of the range of RBF function action. Moreover, the flexible state stability control issue for the hypersonic vehicle should be considered in the controller design.

References

[1] KRSTIC M, KANELLAKOPOULOS I, KOKOTOVIC P V.

Nonlinear and adaptive control design. New York: Wiley, 1995.
[2] BU X W, WU X Y, CHEN Y X, et al. Adaptive backstepping control of hypersonic vehicles based on nonlinear disturbance observer. Journal of National University of Defense Technology, 2014, 36(5): 44 – 49. (in Chinese)
[3] XU B, SUN F C, YANG C G, et al. Adaptive discrete-time controller design with neural network for hypersonic flight vehicle via back-stepping. International Journal of Control, 2011, 84(9): 1543 – 1552.
[4] CHEN W S, JIAO L C. Adaptive tracking for periodically time-varying and nonlinearly parameterized systems using mul-tilayer neural networks. IEEE Trans. on Neural Networks. 2010, 21(2): 345 – 351.
[5] CHEN W S, JIAO L C, LI J, et al. Adaptive NN backstepping output-feedback control for stochastic nonlinear strict-feedback systems with time-varying delays. IEEE Trans. on Systems, Man, and Cybernetics, 2010, 40(3): 939 – 950.
[6] WU J, LI J, CHEN W S. Semi-globally/globally stable adaptive NN backstepping control for uncertain MIMO systems with tracking accuracy known a priori. Journal of Franklin Institue 2014, 351(12): 5274 – 5309.
[7] XU B, SHI Z K, YANG C G, et al. Composite neural dynamic surface control of a class of uncertain nonlinear systems instrict-feedback form. IEEE Trans. on Cybernetics, 2014, 14(12): 2626 – 2634.
[8] DARBHA S, HEDRICK J K, YIP P P, et al. Dynamic surface control for a class of nonlinear systems. IEEE Trans. on Automatic Control, 2000, 45(20): 1893 – 1899.
[9] SONG B, HEDRICK J K. Dynamic surface control of uncertain nonlinear systems: an LMI approach. New York: Springer-Verlag, 2011.
[10] HUANG J T. Global adaptive neural dynamic surface control of strict-feedback systems. Neurocomputing, 2015, 165(12): 403 – 413.
[11] PARKER J T, SERRANI A, YURKOUICH S, et al. Control-oriented modeling of an air-breathing hypersonic vehicle. Journal of Guidance, Control, and Dynamics, 2007, 30(3): 856 – 869.
[12] XU B. Robust adaptive neural control of flexible hypersonic flight vehicle with dead-zone input nonlinearity. Nonlinear Dynamic, 2015, 80(5): 1509 – 1520.
[13] ATAEI A, WANG Q. Non-linear control of an uncertain hypersonic aircraft model using robust sum-of-squares method. IET Control Theory and Applications, 2012, 6(2): 203 – 215.
[14] XU B, SHI Z K, YANG C G, et al. Neural control of hypersonic flight vehicle model via time-scale decomposition with throttle setting constraint. Nonlinear Dynamic, 2013, 73(3): 1849 – 1861.
[15] XU B, GAO D X, WANG S X. Adaptive neural control based on hgo for hypersonic flight vehicles. Science China: Information Sciences, 2011, 54(3): 511 – 520. (in Chinese)
[16] SHI X C, LIM C C, SHI P, et al. Adaptive neural dynamic surface control for nonstrict-feedback systems with output dead-zone. IEEE Trans. on Neural Networks & Learning Systems, 2018, 12(23): 99 – 105.
[17] POLYCARPOU M M. Stable adaptive neural control scheme for nonlinear systems. IEEE Trans. on Automatic Control, 1996, 41(3): 447 – 451.
[18] LIU L H, ZHU J W, TANG G J, et al. Diving guidance via feedback linearization and sliding mode control. Aerospace Science and Technology, 2015, 41: 16 – 23.
[19] WANG N, WU H N, GUO L. Coupling-observer-based nonlinear control for flexible air-breathing hypersonic vehicles. Nonlinear Dynamic, 2014, 78(3): 2141 – 2159.
[20] HU C, LIU Y. Fuzzy adaptive nonlinear control based on dynamic surface control for hypersonic vehicle. Control Decision, 2013, 28(12): 1849 – 1854. (in Chinese)
[21] ZHAO H W, LIANG Y, YANG X X, et al. Prescribed performance fine attitude control for a flexible hypersonic vehicle with unknown initial errors. Asian Journal of Control, 2018, 20(6): 2357 – 2369.
[22] PU Z Q, YUAN R Y, TAN X M, et al. An integrated approach to hypersonic entry attitude control. International Journal of Automation and Computing, 2014, 11(1): 39 – 50.
[23] CAO W, HAN Y F. Flat-plate hypersonic boundary-layer flow instability and transition prediction considering air dissociation. Applied Mathematics and Mechanics, 2019, 40(5): 719 – 736.
[24] BU X W, HE G J, WANG K. Tracking control of air-breathing hypersonic vehicles with non-affine dynamics via improved neural back-stepping design. ISA Transactions, 2018, 75: 88 – 100.
[25] XU B. Disturbance observer-based dynamic surface control of transport aircraft with continuous heavy cargo airdrop. IEEE Trans. on Systems, Man, and Cybernetics: Systems, 2017, 47(1): 1 – 10.
[26] XU B, WANG Y, WANG Z W, et al. An effective approach to detecting both small and large complexes from protein-protein interaction networks. BMC Bioinformatics, 2017, 18(S12): 419.
[27] YANG C G, TENG G, XU B. Global adaptive tracking control of robot manipulators using neural networks with finite-time learning convergence. International Journal of Control Automation & Systems, 2017, 15(11): 1 – 9.
[28] YANG C G, JIANG Y M, HE W. Adaptive parameter estimation and control design for robot manipulators with finite-time convergence. IEEE Trans. on Industrial Electronics, 2018, 25(11): 99 – 108.
[29] XU B, QI Z, PAN Y P. Neural network based dynamic surface control of hypersonic flight dynamics using small-gain theorem. Neurocomputing, 2016, 173(3): 690 – 699.
[30] SUN F C, PAN Y P, CHEN B D. Disturbance observer based composite learning fuzzy control of nonlinear systems with unknown dead zone. IEEE Trans. on Systems, Man, and Cybernetics: Systems, 2017, 47(8): 1854 – 1862.

Biographies

ZHAO Hewei was born in 1985. He received his Ph.D. degree in control science and engineering from Naval Aeronautical Engineering Institue in 2017. He is currently working as a lecturer in Naval Aviation University. His research interests include nonlinear control and intelligent control. His main areas of research are control system design for hypersonic vehicle, and nonlinear control method application for aircraft control system design.
E-mail: zhwsdyt@163.com

LI Rui was born in 1986. She received her M.S. degree in economic management from Yantai University in 2017. She is a lecturer in the Wenjing College, Yantai University. Her research interests include the intelligent algorithm and the neural network method. Her main areas of research is application of the intelligent algorithm in the evaluation method.
E-mail: lirui2016@126.com